PCCP
Physical Chemistry Chemical Physics

Accepted Manuscript

This article can be cited before page numbers have been issued, to do this please use: M. Van Daele, M. Griffiths, M. M. Minjauw, S. Barry, C. Detavernier and J. Dendooven, *Phys. Chem. Chem. Phys.*, 2020, DOI: 10.1039/C9CP06855D.

View Article Online
DOI: 10.1039/C9CP06855D

PCCP

ARTICLE TYPE

Cite this: DOI: 00.0000/xxxxxxxxxx

Reaction mechanism of the Me_3AuPMe_3-H_2 plasma-enhanced ALD process†

Michiel Van Daele,[a] Matthew B. E. Griffiths,[b] Matthias M. Minjauw,[a] Seán T. Barry,[b] Christophe Detavernier,[a] and Jolien Dendooven*[a]

Received Date
Accepted Date

DOI: 00.0000/xxxxxxxxxx

The reaction mechanism of the recently reported Me_3AuPMe_3 - H_2 plasma gold ALD process was investigated using *in-situ* characterization techniques in a pump-type ALD system. *In-situ* RAIRS and *in-vacuo* XPS measurements confirm that the CH_3 and PMe_3 ligands remain on the gold surface after chemisorption of the precursor, causing self-limiting adsorption. Remaining surface groups are removed by the H_2 plasma in the form of CH_4 and likely as PH_xMe_y groups, allowing chemisorption of new precursor molecules during the next exposure. The decomposition behaviour of the Me_3AuPMe_3 precursor on a Au surface is also presented and linked to the stability of the precursor ligands that govern the self-limiting growth during ALD. Desorption of the CH_3 ligands occurs at all substrate temperatures during evacuation to high vacuum, occurring faster at higher temperatures. The PMe_3 ligand is found to be less stable on a gold surface at higher substrate temperatures and is accompanied by an increase in precusor decomposition on a gold surface, indicating that the temperature dependent stability of the precursor ligands is an important factor to ensure self-limiting precursor adsorption during ALD. Remarkably, precursor decomposition does not occur on a SiO_2 surface, *in-situ* transmission absorption infrared experiments indicate that nucleation on a SiO_2 surface occurs on Si-OH groups. Finally, we comment on the use of different co-reactants during PE-ALD of Au and we report on different PE-ALD growth with the reported O_2 plasma and H_2O process in pump-type versus flow-type ALD systems.

1 Introduction

The development of atomic layer deposition (ALD) processes for gold has proven to be challenging compared to its chemical vapour deposition (CVD) counterpart. This is reflected by the existence of only three gold ALD processes.[1–3] In contrast there exists a large list of CVD processes using several different types of gold complexes to deposit gold films.[4] In this paper we will focus on the recently introduced ALD processes that make use of trimethylphosphinotrimethylgold(III) (Me_3AuPMe_3) as the gold precursor which has been used as a CVD precursor before.

The first Me_3AuPMe_3 based ALD processes uses O_2 plasma and H_2O as the co-reactants and was reported by Griffiths et al.[1] They were able to deposit metallic gold in a flow-type reactor, at a deposition temperature of 120°C with a growth rate of 0,05 nm per cycle. A combustion type reaction was proposed as the reaction mechanism:

$$Me_3P{-}AuMe_3 + O^* \longrightarrow Au_2O_3 + P_2O_5 + 6CO_2 + 9H_2O$$

with O* the oxygen radicals formed in the plasma. The gold oxide is then slowly reduced to metallic gold:

$$Au_2O_3 \longrightarrow 2Au^0 + \tfrac{3}{2}O_2$$

Without the H_2O exposure the films contained a lot of phosphorous impurities and a mixture of Au oxidation states. Adding the H_2O exposure results in the removal of the phosphorous impurities and a neutral oxidation state for the gold. They proposed that the addition of water leads to the formation of phosphoric acid which is removed during the purge step:

$$P_2O_5 + 3H_2O \longrightarrow 2H_3PO_4$$

The removal of the phosphate layer seems to aid the reduction of the gold oxide to gold metal.

The other Me_3AuPMe_3 based ALD process uses H_2 plasma as the co-reactant.[3] This process allows the deposition of metallic gold over a broad temperature range from 50 °C to 120 °C with a growth rate of 0,030±0,002 nm per cycle. The reaction mechanism has not been studied in detail. What is known is that the used precursor does not readily decompose on SiO_2 sub-

[a] Ghent University, Department of Solid State Sciences, CoCooN Research Group, Krijgslaan 281/S1, Ghent 9000, Belgium. E-mail: jolien.dendooven@ugent.be*
[b] Carleton University, Department of Chemistry, 1125 Colonel By Drive, Ottawa K1S 5B6, Canada.

† Electronic Supplementary Information (ESI) available: [details of any supplementary information available should be included here]. See DOI: 10.1039/cXCP00000x/

View Article Online
DOI: 10.1039/C9CP06855D

strates over the reported temperature range, while it does exhibit some decomposition on a gold seed layer. A given number of gold exposures, without co-reactant, results in a deposited gold thickness that is $1/6^{th}$ of the amount of gold deposited when an equal amount of ALD cycles would be used. Experimental evidence to support the steady growth reaction mechanism for the Me_3AuPMe_3 - H_2 plasma process is lacking. The existing literature (CVD, surface science, decomposition studies) concerning the use of the Me_3AuPMe_3 precursor provides a starting point to identify the reaction mechanism that occurs during the Me_3AuPMe_3 - H_2 plasma ALD process. Understanding possible decomposition pathways of the used precursor can provide valuable information about how the chemical reactions can occur on a substrate.

The existing decomposition investigations of Au(I) and Au(III) compounds, similar to the Me_3AuPMe_3 molecule, are limited to the study of the liquid phase, which nonetheless provide important insights in the chemistry of these gold compounds. Gold compounds of the form RAuPR'$_3$ and R$_3$AuPR'$_3$ (with R = methyl, ethyl; R' = methyl, ethyl, phenyl) generally decompose into coupled R-R species, elemental gold, and the phosphine ligand.[5–8] The decomposition pathway usually starts with the elimination of two neighbouring alkyl groups, resulting in the formation of R-R and RAuPR'$_3$ species. It was found that adding the phosphine ligand to the liquid results in retardation of the decomposition, indicating that for liquids the rate-limiting step in the decomposition of RAuPR'$_3$ molecules is the loss of the phosphine ligand. Davidson et al. reported laser induced CVD of gold tracks using $MeAuPMe_3$, $MeAuPEt_3$, and $EtAuPEt_3$ using an argon ion laser at 257 nm.[9] The elemental composition and inclusion of precursor ligands on the surface was studied using laser ionization microprobe analysis. They observed the presence of chemisorbed PMe_3 species on the gold surface, which remained present on the surface for prolonged periods of time under high vacuum conditions. They inferred that the Au-Me surface species were less stable compared to the Au-PMe_3 surface species. In addition they found indications for the non-dissociative adsorption of $MeAuPMe_3$ on the gold surface. These observations are interesting for elucidating the reaction mechanism of Me_3AuPMe_3 and $MeAuPMe_3$ based processes on gold surfaces during gold deposition.

The origin of the precursor decomposition on a gold surface and its temperature dependence will be investigated in this work, understanding this behaviour is vital for the implementation of this process as it can have a large effect on the steady growth behaviour of the process. *In-situ* characterization techniques will be used in this paper to provide more insight into the reaction mechanism of the Me_3AuPMe_3 - H_2 plasma gold ALD process. This will be done for the steady growth regime on a Au surface. In addition, we shed light on the surface species on which nucleation on an oxide surface can occur. Finally, we will compare the use of different co-reactants in the PE-ALD process and report on the difference in properties of the deposited films.

2 Experimental Section

A home-built pump type ALD reactor, with a base pressure of $2x10^{-6}$ mbar, is used to carry out all atomic layer depositions, unless stated otherwise.[3] The Me_3AuPMe_3 precursor ($\geq$95% purity) is synthesised *via* the method used by Griffiths *et al.*[1] The $(CD_3)_3Au(PMe_3)$ precursor ($\geq$95% purity, and >99% deuteration) is synthesised as described in the paper of Shaw and Tobias.[10] The purity of the precursor liquids is verified by NMR measurements (see Supporting Information). The precursor liquids are kept in glass containers, heated to 50°C and the delivery lines are heated to 55°C. Argon is used as a carrier gas for the precursors during all depositions. The flow of the carrier gas is adjusted to reach a pressure of $6x10^{-3}$ mbar, when pulsing the precursor in the chamber. The precursor exposures during the atomic layer depositions are carried out by injecting the Me_3AuPMe_3 vapour after closing the gate valve between the turbomolecular pump and the reactor chamber. By varying the injection time, the pressure during the pulse varied between $6x10^{-3}$ mbar and 5 mbar. H_2 plasma (20% H_2 in argon) is used as the reactant for all depositions. The H_2 gas is introduced through the plasma column mounted on top of the chamber and the flow of H_2 gas is limited by a needle valve to obtain a chamber pressure of $6x10^{-3}$ mbar for all depositions. A 13,56 MHz RF generator (Advanced Energy, Model CESAR 136) and a matching network are used to generate an inductively coupled plasma in the plasma column. For all experiments a plasma power of 200 W is used and the impedance matching parameters are adjusted to minimise the reflected power. The substrates used are pieces of p-type silicon (100) with native silicon oxide or 10 nm sputtered Au films on p-type silicon (100). The samples are mounted directly on a heated copper block. The temperature of the copper block is adjusted with a PID controller. The chamber walls are heated to 90°C for all experiments unless stated otherwise.

In this work films deposited using a home-built pump type reactor are compared to films deposited using a commercial flow-type reactor. The major differences between both reactor-types are the used operating pressures and how the purge step between precursor and co-reactant exposures is implemented. Typical operation pressures of a flow-type reactor are of the order of 1 mbar, while a pump-type reactor can reach these pressures during an exposure it usually needs to have a base pressure on the order of 10^{-6} mbar to avoid CVD side reactions. In pump-type reactors the purge step is achieved by lowering the pressure in the chamber to the base pressure which removes the gas-phase molecules in the reactor chamber, while a flow-type reactor uses an inert gas to flush/purge the gas-phase molecules from the reactor chamber.

To study the ALD reaction mechanism, *in-situ* infrared spectroscopy, *in-vacuo* X-ray photoelectron spectroscopy (XPS), mass spectrometry. The infrared measurements are carried out with a Vertex 70V from Bruker and a medium band mercury cadmium telluride (MCT) detector cooled with liquid nitrogen. The infrared measurements can be performed in two different geometries, either in reflection or in transmission. For the Reflection Absorption Infra-Red Spectroscopy mode (RAIRS), a thick gold seed layer of 60 nm is used to avoid nucleation effects and to ensure proper reflection of the IR beam.[11] *In-vacuo* XPS measurements were performed with a Thermo Scientific Theta Probe XPS instrument on an ALD-XPS cluster.[12] Using this cluster it is possible to perform through-vacuum transfer of samples from the ALD

View Article Online
DOI: 10.1039/C9CP06855D

chamber (10^{-7} mbar) to the XPS analysis chamber (10^{-10} mbar) in less than 60 seconds. *In-situ* mass spectrometry experiments are carried out using a Hiden HPR-30 mass spectrometer, 70 eV electron impact ionisation and a quadrupole mass filter combined with a Faraday detector. The reactor is loaded with ~2 grams of alumina powder with a diameter of $1\mu m$, providing an estimated surface area of $3m^2$. The tube between the ALD chamber has a length of 1 m and a width of 4 cm and is heated to 90°C to avoid cold spots. The connection between the ALD chamber and fine valve has a diameter of 10 cm (the fine valve is located between the chamber and the turbomolecular pump). The pressure in the QMS chamber during the experiments was $\sim 10^{-7}$ mbar. The reactor and powder are pretreated with 100 Au ALD cycles before performing the QMS measurements.

Several *ex-situ* measurement techniques are used to determine the physical properties of the deposited Au films. Thickness determination *via* X-ray reflectivity (XRR) measurements is done on a diffractometer (Bruker D8) equipped with a copper source (Cu Kα radiation) and a scintillator point detector. However, because the Au ALD films are generally too rough for accurate thickness determination with XRR, X-ray fluorescence (XRF) measurements are used to determine an equivalent film thickness based on a calibration curve of sputtered gold films. XRF measurements are performed using a Mo X-ray source and an XFlash 5010 silicon drift detector, respectively placed at an angle of 45° and 52° with the sample surface. An integration time of 200 s is used to acquire the fluorescence spectra. *Ex-situ* XPS is used to determine the chemical composition and binding energy of the deposited films. The XPS measurements are carried out in the same tool that is used for *in-vacuo* XPS. The X-rays are generated using a monochromatic Al source (Al Kα). To etch the surface of the deposited films an Ar^+ ion gun is used at an acceleration voltage of 3 keV and a current of 2 μA.

3 Results and Discussion

3.1 Precursor saturation and decomposition

The saturation behaviour of the Me_3AuPMe_3 - H_2 plasma ALD process was demonstrated in the previous work.[3] It is important to consider the precursor supply during the saturation experiments as the precursor dose in the chamber will be dependent on the vapour content in the precursor container, which is carried to the ALD reactor in a flow of Argon. The amount of vapour in the container and thus the partial pressure of the precursor during the exposure depends on the container temperature, the exact pulse and purge sequence and the amount of liquid precursor in the container. As long as the precursor dose is sufficient to achieve saturation in the ALD process, these variations will not have impact on the ALD growth per cycle. On the other hand, a too limited buildup of vapour in the container may also invoke an apparent saturated growth behaviour. To rule out the latter, additional ALD saturation experiments were performed at different substrate temperatures for which two precursor containers were used simultaneously during the precursor exposures. The obtained GPC's of these experiments (red diamonds) and the previously reported GPC of the ALD process (black squares) are shown in Figure,1 as a function of substrate temperature. At 50°C and 90°C the GPC showed no increase with respect to the expected GPC of the ALD process, verifying the previously reported saturating behaviour of the ALD process. However, at 120°C the GPC was doubled when two precursor containers were used, indicating that at this substrate temperature the ALD process is dominated by decomposition and that its growth is governed by the precursor supply.

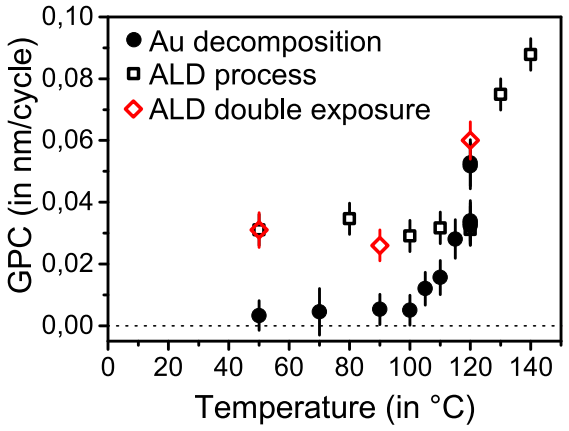

Fig. 1 Decomposition of the Me_3AuPMe_3 molecule (black dots) as a function of substrate temperature and the reported GPC for the gold PEALD process using 1 precursor container (black squares) and 2 precursor containers simultaneously (red diamonds). The decomposition experiments were performed on gold seed layers, using 20 second precursor exposures.

The observed saturating behaviour of the ALD process requires that the surface will get covered by the precursor ligands during the Me_3AuPMe_3 exposure, preventing further precursor adsorption. However, as we reported previously, this process exhibits a minor decomposition component on gold substrates, which we attributed to slow decomposition of the surface ligands.[3] The double precursor container experiments indicate that between a substrate temperature of 90°C and 120°C this minor decomposition component increases in magnitude and heavily influences the growth behaviour at 120°C. Additional experiments were performed to investigate the onset temperature and evolution of this precursor behaviour. This was done by exposing gold seed layers to the Me_3AuPMe_3 vapour only (without co-reactant) at temperatures spanning the entire ALD temperature window (50°C-120°C). While these experiments are not real ALD processes, the observed increase in gold thickness was divided by the number of used precursor exposures and expressed as GPC as a function of substrate temperature in Figure 1 (black dots). The decomposition curve shows that there are two regions with a threshold substrate temperature at 100°C. Below the threshold the decomposition is limited to the previously reported value of 0,005 nm per cycle and above a substrate temperature of 100°C the decomposition component increases with the substrate temperature. At 120°C the decomposition component becomes larger than the expected GPC of the ALD process with a large spread on the obtained GPC, most likely due to differences in precursor supply. The observed Au decomposition curve indicates that the previ-

View Article Online
DOI: 10.1039/C9CP06855D

ously reported upper limit of the ALD temperature window needs to be lowered from 120°C to 100°C.

No precursor decomposition is observed on SiO_2 substrates for temperatures below 120°C. This suggests that the observed decomposition on a gold substrate is not due to thermal decomposition of the precursor itself, but depends on how the precursor and its ligands interact with the gold surface. Therefore, the surface species need to be identified and their stability on the surface investigated.

3.2 Surface species

Using *in-situ* Reflection Absorption Infrared Spectroscopy (RAIRS) it is possible to determine which surface groups are present after each precursor or reactant exposure. To this end, we employed *in-situ* RAIRS measurements on a sputtered gold seed layer (60 nm), at a substrate temperature of 90°C. In addition to the use of the regular precursor molecule (Me_3AuPMe_3) we also performed experiments using a partially deuterated molecule in which the methyl groups attached to the gold atom were replaced by deuterated methyl groups ($((CD_3)_3Au(PMe_3))$), where the PMe_3 ligand remained unaltered. The spectra measured after each exposure in the ALD cycle were subtracted from each other to obtain differences in absorption that are related to the addition/removal of surface species after each exposure and the average of 10 spectra was taken to improve the signal to noise ratio. The obtained difference spectra for both precursor variants are displayed in Figure 2. After the precursor exposure, peaks appear for the vibration modes of methyl and trimethylphosphine (TMP, PMe_3) surface groups, originating from the precursor ligands. Zooms of the CH-stretching, CD-stretching, and fingerprint regions after a precursor exposure are displayed in Figure 2 a-c, assignment of the peaks can be found in Table 1. The C-H stretching region (Figure 2a) has the same four peaks (1-4) for both gold precursor variants. For the deuterated precursor ($((CD_3)_3Au(PMe_3))$) it is expected that these peaks originate exclusively from the TMP ligand, while for the regular precursor (Me_3AuPMe_3) contributions from both the TMP and methyl ligands are expected. The similarity between both spectra indicates that these peaks mainly originate from the TMP ligand. It is hence difficult to uniquely distinguish between the C-H stretching modes of the TMP ligand and the methyl groups, in turn motivating the use of the partially deuterated molecule. The C-D stretching region (Figure 2b) shows a clear contribution from C-D species (5 and 6) for the deuterated precursor, indicating that Au-CD_3 species are present on the gold surface after the precursor exposure. The zoom of the fingerprint region is shown in Figure 2c. The methyl deformation and rocking modes (7, 8, 10) originate from the TMP ligand and in combination with the PC_3 stretching mode (11) give a good indication that the TMP ligands remain intact. Remarkable is the lack of vibration modes between 1250 $cm^{-1}$and 1150 cm^{-1} where methyl deformation modes of Au-$(CH_3)_3$ species are expected. On the other hand, there is a feature present in the spectrum of the regular precursor at 1100 cm^{-1}(9), which might originate from single methyl species bound to a gold atom.[13] This feature disappears for the deuterated precursor and a new feature appears at a lower position (9') most likely from deuterated methyl species bound to the gold surface.

Peak	Position (in cm^{-1})	Vibration mode
1	2968	$\nu_{as}(CH_3)$-[P]
2	2958	$\nu_{as}(CH_3)$-[P/Au]
3	2901	$\nu_{s}(CH_3)$-[P/Au]
4	2887	$\nu_{s}(CH_3)$-[P/Au]
5	2218	$\nu_{as}(CD_3)$-Au
6	2110 and 2086	$\nu_{s}(CD_3)$-Au
7	1422	$\delta_{as}(CH_3)$-[P]
8	1285 and 1301	$\delta_{s}(CH_3)$-[P]
9	1100	$\delta_{as}(CH_3)$-[Au]
9'	778	$\delta_{as}(CD_3)$-[Au]
10	954	$\rho(PCH_3)$
11	667	$\nu_{s}(PC_3)$

Table 1 Position and assigned vibration modes of the observed features in the FTIR difference spectra displayed in Figure 2. The assignment of these peaks is based on a reference IR spectrum for the Me_3AuPMe_3 molecule and for the PMe_3 ligand.[13–15] (ν stretching, δ deformation, ρ rocking, as = asymmetric, s = symmetric)

The symmetrical difference spectra for the precursor and reactant exposure indicate that the H_2 plasma exposure is able to remove all of the surface groups that are added during the precursor exposures. It is possible that Au-H surface species are formed during the H_2 plasma exposure, for which vibration modes are expected around 2230-2170 cm^{-1} and 1642 cm^{-1}.[16] However, no absorption is visible in those regions after a H_2 plasma exposure, indicating that any formed Au-H species remain below the detection limit of our setup. Furthermore, it is unlikely that a significant amount of Au-H species would be stable for prolonged periods of time on a large gold surface and at temperatures above −148°C.[17,18]

To verify that the H_2 plasma is able to remove the CH_3 and PMe_3 groups from the surface an *in-vacuo* XPS experiment was performed on a gold seed layer. The used sample was a silicon oxide substrate, on which a thick gold layer was sputtered. Before performing the *in-vacuo* experiment the sample was coated with 300 gold ALD cycles at a substrate temperature of 90°C. This was done to eliminate the measurement of an XPS signal from the underlying sputtered gold layer. After the ALD deposition was finished, ending with a H_2 plasma, the sample was transferred within 1 minute from the ALD chamber to the XPS analysis chamber without breaking vacuum. The measured P2p, C1s, and Au4f peaks are show in Figure 3. The Au4f peaks show that the gold is present in one oxidation state. The Au4f 5/2 peak was set to 84,0 eV and used to calibrate the spectra. It is clear that no P2p or C1s signals were detected on the sample after the H_2 plasma pulse, indicating that the CH_3 and PMe_3 groups are removed from the surface by the H_2 plasma, corroborating the RAIRS measurements.

In-vacuo XPS measurements were also performed after the precursor exposure and this was done at four substrate temperatures: 50°C, 90°C, 120°C, and 140°C. The obtained Au4f, P2p, and C1s peaks of these experiments are displayed in Figure 4. It is clear

View Article Online
DOI: 10.1039/C9CP06855D

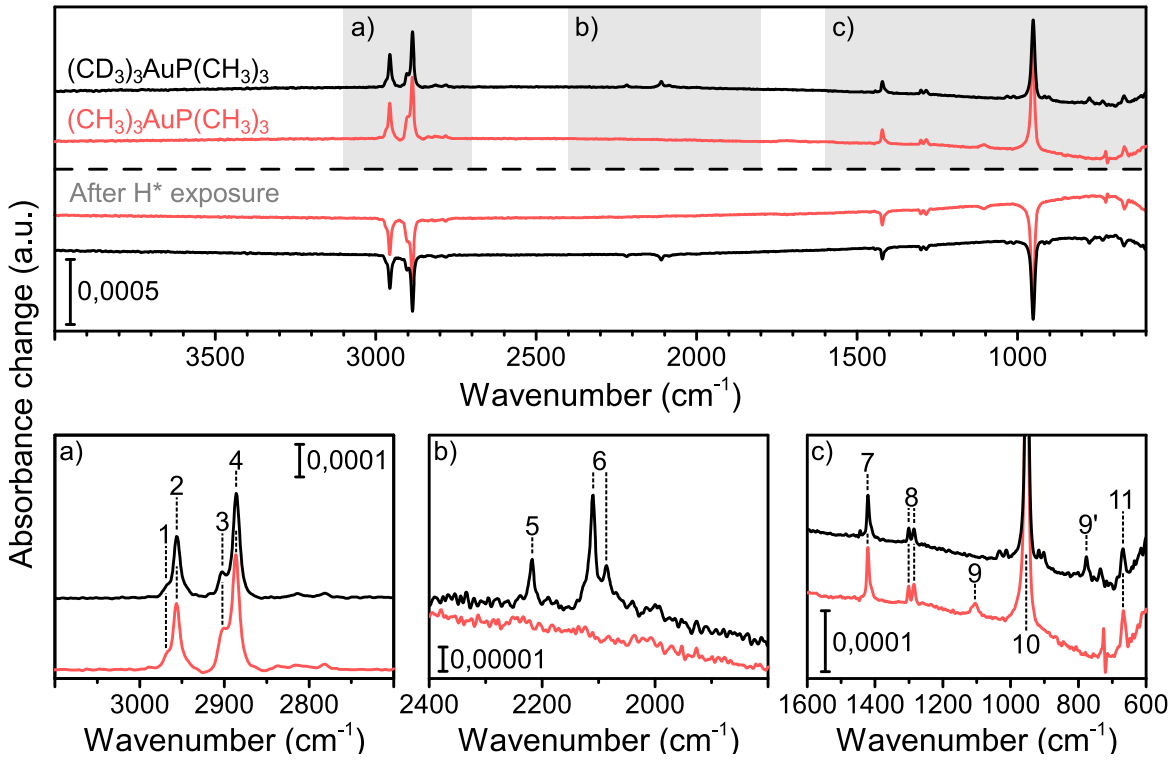

Fig. 2 Difference spectra for the Me_3AuPMe_3-H_2 plasma and $(CD_3)_3Au(PMe_3)$-H_2 plasma ALD processes. Thick sputtered gold layers (60 nm) were used as substrates and depositions were performed at a substrate temperature of 90°C. The regions marked by a), b), and c) are zooms of the CH-stretching, CD-stretching, and fingerprint regions, respectively, after a precursor exposure. Assignments for the marked peaks can be found in Table 1.

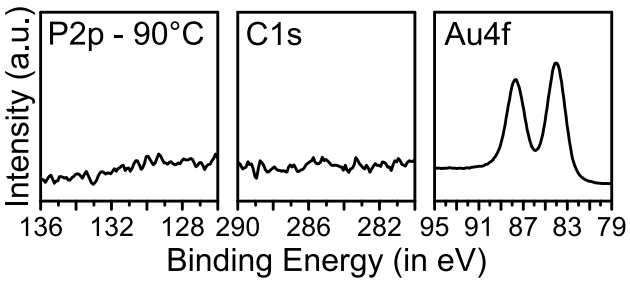

Fig. 3 P2p, C1s, Au4f peaks measured by XPS on a gold seed layer after performing a gold ALD process ending with a H_2 plasma exposure. The deposition was performed at a substrate temperature of 90°C. After ending the ALD process the sample was transferred within 1 minute from the ALD chamber to the XPS analysis chamber without breaking vacuum.

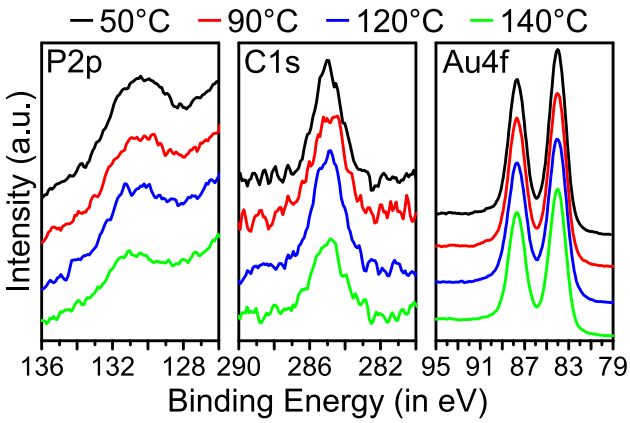

Fig. 4 P2p, C1s, Au4f peaks measured by XPS on a gold seed layer after performing a gold ALD process ending with a precursor exposure. Depositions were performed at a substrate temperature of 50°C, 90°C, 120°C, and 140°C. After ending the ALD process the samples were transferred as quickly as possible from the ALD chamber to the XPS analysis chamber without breaking vacuum.

View Article Online
DOI: 10.1039/C9CP06855D

	Substrate Temp.	Au4f (atom %)	C1s (atom %)	P2p (atom %)	C/P
a)	50°C	86 ± 1	10 ± 1	4 ± 1	2,5
	90°C	88 ± 1	9 ± 1	3 ± 1	3
	120°C	87 ± 1	10 ± 1	3 ± 1	3,3
	120°C	89 ± 1	8 ± 1	3 ± 1	2,7
	140°C	91 ± 1	7 ± 1	2 ± 1	3,5
b)	50°C	84 ± 1	12 ± 1	4 ± 1	3
	90°C	83 ± 1	14 ± 1	3 ± 1	4,7
	120°C	85 ± 1	12 ± 1	3 ± 1	4,3
	140°C	84 ± 1	13 ± 1	3 ± 1	4,3

Table 2 XPS determined atomic concentrations of Au, C, P, and the C/P ratio of Me_3AuPMe_3 exposures on a gold seed layer at different temperatures. The samples were transferred from the ALD chamber to the XPS analysis chamber without breaking vacuum. a) Samples transferred immediately after the final precursor exposure. b) Samples transferred 18 hours after the final precursor exposure.

that in all cases the Au surface remains in a metallic state and that there is carbon and phosphorous present from the CH_3 and TMP precursor ligands. The atomic concentrations and C/P ratios of these samples and of samples that were transferred after an 18 hour waiting period are displayed in Table 2a and Table 2b, respectively. The latter samples remained on the heated copper block for the entire waiting period. The C/P ratio yields information about the ratio of CH_3 to TMP species that are present on the surface. For the samples that were transferred immediately there is an increase in the atomic concentration of the Au4f peak with increasing temperature, which indicates that the amount of C and P on the surface is lower at higher temperatures. A C/P ratio of 6 would indicate that all of the precursor ligands remain on the surface, while lower values indicate the partial removal of the [Au]-CH_3 species from the surface with a value of 3 indicating that only the TMP ligand remains on the surface. The C/P ratios fluctuate between 2,5 and 3,5 which is in agreement with the presence of TMP groups on the surface and only a minority component of CH_3 species, which are contributed by the gold centre. The amount of phosphorous present on the surface is the largest at 50°C and at the other temperatures there is roughly a quarter to a half less phosphorous present. The amount of phosphorous is directly linked to the amount of TMP on the surface and this result suggests that TMP is less stable on the gold surface with increasing substrate temperature, which is supported by surface science literature, based on temperature programmed desorption (TPD) experiments of dimethylphenylphosphine from Au(111) surfaces.[19] The TPD experiments indicated the onset of desorption of chemisorbed dimethylphenylphosphine at a substrate temperature of 60°C with the peak of desorption above a substrate temperature of 170°C. For the samples that were transferred after an 18 hour waiting period (Table 2b), no significant change in the P2p atomic concentration is observed, but an increase in the carbon signal is present for all of them. The phosphorous signal indicates that at least a fraction of the TMP ligands remains on the surface. Adventitious carbon contaminating the surface can explain the increase in the carbon signal.

3.2.1 Stability of surface species

Reports in literature indicate that phosphorous based molecules can form strong bonds with a gold surface,[19–24] in line with the *in-situ* RAIRS and *in-vacuo* XPS measurements, confirming the presence of TMP groups on the gold surface after the precursor exposure. The *in-situ* RAIRS data also revealed the presence of CH_3 groups on the gold surface. However, the C/P ratios determined from the *in-vacuo* XPS measurements indicate that the CH_3 species are removed from the surface and over time mainly the TMP ligands remain. It needs to be noted that the measurement time of both methods differs significantly. Each IR measurement is completed within 2 minutes after the precursor exposure, while each *in-vacuo* XPS experiment lasted for several hours. To bridge this gap, we performed several RAIRS measurements over the course of an hour after a precursor exposure. This was done at a substrate temperature of 90°C and 120°C. The obtained results can be seen in Figure 5. The normalized intensity of the main TMP rocking mode (954 cm^{-1}) is plotted as a function of time after precursor exposure in Figure 5a. The intensity decays over time for both temperatures and this decay occurs faster at 120°C than at 90°C, suggesting that these groups are less stable at higher substrate temperatures. Figure 5b shows the 1250-900 cm^{-1} region of the first two spectra that were obtained during these experiments at 90°C and 120°C. A first thing to note is that the initial spectrum obtained at 90°C shows the [Au]-Me mode at 1100 cm^{-1}, while the spectrum obtained at 120°C does not, indicating that the [Au]-Me groups are less stable at higher substrate temperatures. The second spectrum obtained at 90°C shows that the [Au]-Me vibration mode has decreased to the noise level, indicating that the CH_3 groups quickly desorb from the surface, which is in agreement with the observed *in-vacuo* XPS results.

3.3 Reaction by-products

While the *in-situ* RAIRS and *in-vacuo* XPS data yield information about the surface groups that are present after each exposure, they do not provide information about the reaction by-products that are being formed during the process. In order to study the formed by-products we used *in-situ* quadrupole mass-spectrometry (QMS) during the ALD process. Mass-to-charge ratios for methyl, methane, ethane, PH_x, PMe_x, and H_yPMe_x (x, y = 1-3) were followed. This was done during five ALD cycles, each exposure lasted for 15 seconds with a 15 seconds pump steps between exposures. Three precursor exposures were given before performing the ALD cycles to saturate the surface and after the ALD cycles three H_2 plasma exposures were given. The obtained data for mass to charge ratios 15 (CH_3) and 16 (CH_4) as a function of time is displayed in Figure 6. The signal for the other mass to charge ratios did not exceed the noise level.

The signal for mass 15 is part of the cracking pattern for a pure methane gas. In this case the signals of masses 15 and 16 coincide with the expected ratio for a methane cracking pattern. This indicates that CH_4 groups are formed during the H_2 plasma exposures. While this accounts for the removal of the methyl groups from the surface, it does not reveal how the phosphorous of the PMe_3 ligands is removed from the surface as the signals

View Article Online
DOI: 10.1039/C9CP06855D

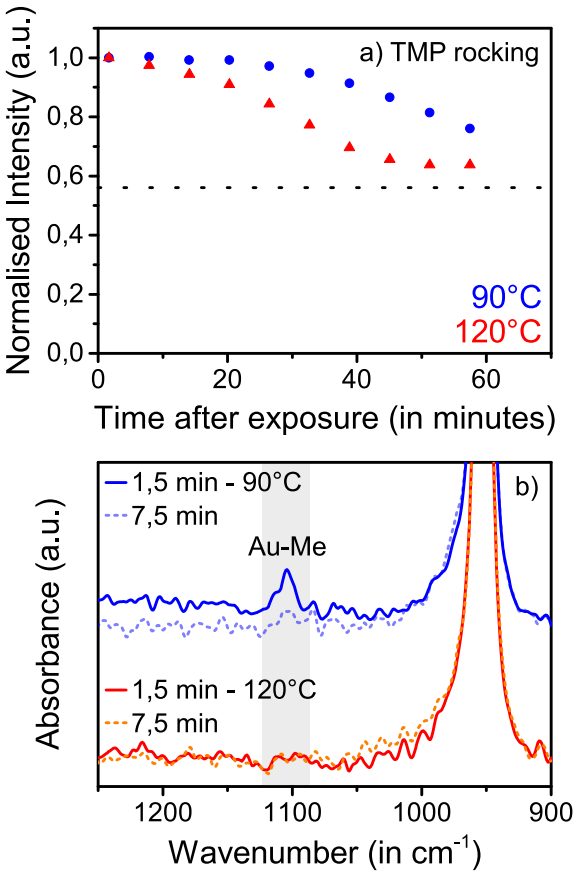

Fig. 5 RAIRS data for a precursor exposure on a thick sputtered gold layer at a substrate temperature of 90°C and 120°C. a) Normalized intensity of the main TMP rocking mode at 954 cm^{-1} as a function of the elapsed time after a precursor exposure. The dotted line represents the normalized intensity at 120°C after 2 hours and 30 minutes. b) fingerprint region, covering the $\delta_{as}(CH_3)$-[Au] deformation mode (grey box, 1100 cm^{-1}) and the main TMP rocking mode. The shown spectra are recorded 30 seconds after the precursor exposure and 6 minutes and 30 seconds after the precursor exposure.

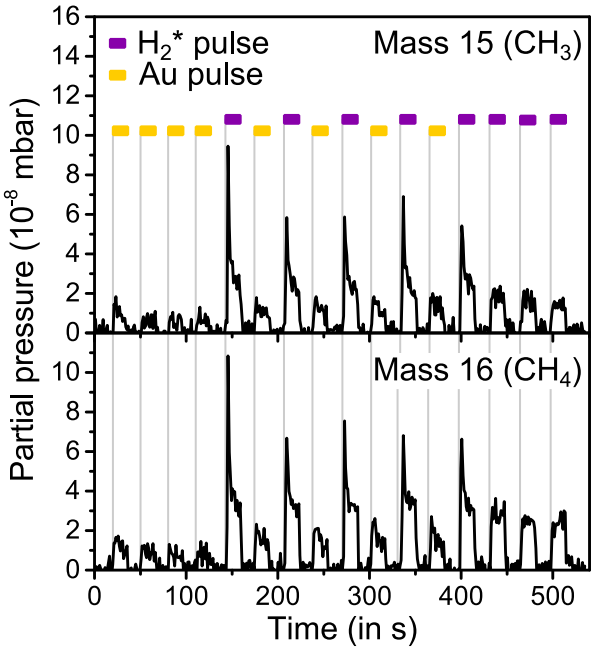

Fig. 6 Mass spectrometry measurements for mass to charge ratios 15 (CH_3) and 16 (CH_4) during a Me_3AuPMe_3 - H_2 plasma process. The data shows 3 precursor pulses, followed by 5 ALD cycles and ending with an additional 3 H_2 plasma pulses. The deposition was carried out using a substrate temperature of 90°C.

for the phosphine and (tri,di)methylphosphine related masses did not exceed the noise level during the exposure. It is possible that they reacted with the side walls of the flexible tube that connects the chamber to the QMS detector and did not reach the QMS detector.

The QMS data also reveal that a minor fraction of CH_4 is formed during the precursor exposure and the ratio of the signals for masses 15 and 16 coincides with the expected ratio for a pure CH_4 gas. This indicates that the observed signal originates from CH_4 groups instead of CH_3 radicals. Otherwise, the signal for mass 15 can be expected to be much larger than the signal for mass 16. There are a few possible explanations for the formation of CH_4: CH_3 ligands on the surface are able to react with hydrogen, either present on the surface or impinging on the surface from residual molecular hydrogen in the chamber. Another possibility is that CH_3 radicals desorb from the surface and pick up a hydrogen atom when colliding with the walls/inlet of the chamber/QMS inlet or residual hydrogen in the chamber. The latter case is less likely as it can be expected that this would lead to a larger signal for CH_3 species, compared to that of CH_4. A final possibility is that CH_3 ligands abstract a hydrogen atom from neighbouring CH_3 ligands, as is the case in the thermal $MeCpPtMe_3$ - O_2 ALD process.[25] It has been observed that Au^+ and Au_2^+ cations are able to dehydrogenate methane to CH_2 and for the Au_2^+ cations the adsorption of multiple methane molecules leads to the formation of ethylene.[26–30] However, larger gold particles are not able to cleave more than one C-H bond of methane and for particles that contain more than 15 Au atoms even the adsorption of methane is not observed.[31]

View Article Online
DOI: 10.1039/C9CP06855D

Interestingly, there is no ethane detected during the precursor exposure, while its formation is to be expected from the decomposition literature of similar liquid gold compounds. The first step in the reduction of Au(III) compounds to Au(0) occurs by alkyl-coupling, causing the removal of two of the CH_3 groups, forming ethane, and reducing the gold atom from a +3 to a +1 oxidation state.[6–8] This is also seen when adsorbing alkyl-halide molecules on gold surfaces with the onset of ethane desorption at −33°C from Au(111) planes and at 27°C from Au(100) planes.[32,33] However, when co-adsorbing CH_3-I with trimethylphosphine on a Au(100) surface the formation of ethane does not occur and instead the CH_3 species desorb as CH_3-radicals above a substrate temperature of 100°C.[33] The removal of CH_3 groups from Au(111) planes can thus occur below 0°C,[32,33] which in our case would mean that the CH_3 groups that are adsorbed during the precursor exposure will quickly be removed from the gold surface. And, as no ethane is detected in the QMS, it is likely that the co-adsorption of trimethylphosphine on Au(111) planes has a similar effect as the co-adsorption on Au(100) planes, preventing the coupling of the alkyl groups on the surface.

3.4 Reaction scheme

Based on the *in-situ* RAIRS, *in-vacuo* XPS, and *in-situ* QMS data it is possible to propose a reaction mechanism for the Me_3AuPMe_3 - H_2 plasma ALD process under steady growth conditions. This reaction scheme is depicted in Figure 7 for three different temperature regimes: T <100°C, 100°C <T <120°C, and T >120°C with the main reaction scheme given by the first temperature regime, the other temperature regimes extend on it to include additional effects that cause the precursor decomposition on a gold surface (see Figure 1).

The first step in the ALD process will be to expose this surface to the Me_3AuPMe_3 molecules, which will physisorb on the surface (step a). After physisorption, the precursor molecules can undergo reactions with the surface and chemisorb. Based on how similar gold molecules behave in a liquid the most likely pathway for chemisorption on the gold surface is by breaking the Au-P bond (step b).[7,8] The *in-situ* RAIRS measurements (Figure 2) show that both CH_3 and PMe_3 ligands remain on the gold surface after chemisorption. The surface coverage with CH_3 and PMe_3 ligands will prevent further adsorption of Me_3AuPMe_3 molecules and cause self-limiting behaviour during the Me_3AuPMe_3 exposure. During the chemisorption step the CH_3 species start to desorb from the surface, most likely in the form of CH_4, as evidenced by the QMS data (step c). Most likely the CH_3 ligands react with residual hydrogen in the chamber or atomic hydrogen that is present on the surface to form CH_4. It is also possible that the CH_3 groups abstract a hydrogen atom from a neighbouring CH_3 group to form CH_4 and leave a CH_2 group on the surface. However, it is expected that this effect only occurs for very small gold particles (less than 15 Au atoms).[31]

The C/P ratio obtained from the *in-vacuo* XPS data shows that this desorption of CH_3 groups occurs at all substrate temperatures. Based on the results from Paul and Bent this is expected for Au(111) planes at the used substrate temperatures, while on

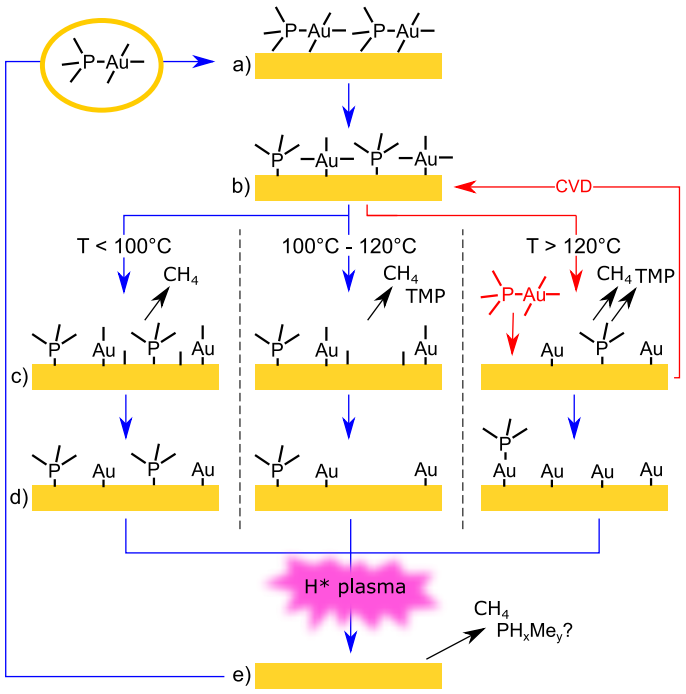

Fig. 7 Schematic drawing of the Me_3AuPMe_3 - H_2 plasma ALD process for different substrate temperatures. (TMP = PMe_3, each dangling bar (-) represents a CH_3 group) a) Physisorption of the precursor on a clean gold surface. b) Initial chemisorption on the surface. c) Desorption of CH_4 and TMP species. d) Final surface state after pumping. e) Removal of remaining surface groups by H_2 plasma.

Au(100) planes this should only occur above a substrate temperature of 100°C.[33] The *in-situ* RAIRS experiments (Figure 5b) indicate that at 90°C there are still CH_3 groups present after several minutes, while they are undetectable at 120°C, showing that the removal of CH_3 species occurs faster at higher temperatures.

The RAIRS and XPS data show that the TMP ligand is rather stable on the gold surface. There are reports of the behaviour of the TMP ligand on a gold surface in literature. Jewell et al. reported that annealing one monolayer of adsorbed TMP on a Au(111) surface to 77°C results in a coverage of 88 % of a monolayer.[23] Temperature programmed desorption experiments of dimethylphenylphosphine on Au(111) indicate an onset of desorption around 77°C, although the maximum of the desorption peak is located above 177°C.[19] In addition, it is expected that in the class of alkylphosphine molecules swapping the phenyl groups with a CH_3 group results in a stronger Au-P bond,[22] which would indicate a higher desorption temperature for TMP compared to dimethylphenylphosphine, meaning that the TMP groups remain stable for a longer period of time at substrate temperatures below 100°C. This is also corroborated by the *in-situ* RAIRS experiments (Figure 5a), showing that while at 90°C the TMP groups are being removed from the surface they remain stable for a rather long time period.

As mentioned in step b of the ALD cycle, it is likely that the chemisorption step involves breaking the Au-P bond, leaving TMP and CH_3 groups on the surface. The stability of these groups has an influence on the observed precursor decomposition be-

View Article Online
DOI: 10.1039/C9CP06855D

haviour (see Figure 1). If these surface species are unstable on the gold surface they will desorb over time and in doing so create additional physisorption sites for precursor molecules, leading to precursor decomposition. Based on the decomposition curve of Figure 1 there are three regions that can be distinguished: T = 50-100°C, T = 100-120°C, and T >120°C, the stability of the surface species for each temperature region is depicted in step c.

Below 100°C only a minor decomposition component is observed and based on the discussion of the RAIRS and XPS data it seems likely that the main desorption component originates from the CH_3 ligands (most likely in the form of CH_4), or at least on the timescale of a single ALD cycle. In addition the coverage of TMP on a gold surface can be expected to be not more than 88 % of a monolayer, which can already account for the most part of the observed decomposition component at this temperature.

For substrate temperatures between 100°C and 120°C the decomposition increases with temperature, surpassing the expected GPC of the ALD process at 120°C. Based on the above discussion, this increase in decomposition as a function of substrate temperature indicates that both CH_3 and TMP are able to desorb in reasonable amounts from the surface within the timescale used for ALD, providing additional adsorption sites for the precursor during the next exposure.

The large and uncontrolled decomposition at substrates temperature above 120°C indicates that the desorption of CH_3 and TMP is able to occur fast enough during the precursor exposure in such a way that during ALD the GPC exceeds the value of 0,03 nm per cycle, which is obtained for saturated reactions below 100°C. The result is that during exposure additional adsorption sites are created for the precursor, which leads to additional deposition of gold on the surface and uncontrolled growth rates at high temperatures. In addition, above 120°C thermal decomposition is expected to occur. [1]

Based on the C/P ratio of 3 determined from the XPS experiments all CH_3 groups will be removed from the surface after the precursor exposure when sufficient time is given and the surface will be covered by a varying amount of TMP molecules, dependant on the substrate temperature (step d). This coverage will determine the amount of adsorption sites for precursor molecules when the surface is again exposed to the precursor, which can explain the observed precursor decomposition curve.

After the precursor exposure the surface is exposed to a H_2 plasma (step e). The plasma removes the contaminating PMe_3 and remaining CH_3 groups from the surface, evidenced by the RAIRS and XPS measurements. Insufficiently long plasma exposures result in the incomplete removal of the precursor ligands, indicated by *ex-situ* XPS measurements on gold films deposited with short plasma exposures, see Supporting Information. This means that after too short of a plasma exposure a part of the precursor adsorption sites are blocked by remaining precursor ligands, which results in a lower GPC for the ALD process. Based on the QMS data the CH_3 species are liberated and converted to CH_4. It is unclear in exactly what form the phosphorous is removed from the surface, as no phosphorous containing species were detected in the QMS measurements. However, it is likely that it is removed as methylphosphine or phosphine species (PH_xMe_y, x,y=0-3). The end result is expected to be a clean gold surface, because there was no direct evidence of atomic hydrogen on the gold surface. Although it cannot be excluded that a small concentration of atomic hydrogen remains on the surface, aiding with the removal of the CH_3 species as CH_4 in step c of the reaction. After the plasma exposure the ALD cycle can start over on this clean gold surface.

3.5 Nucleation on SiO_2

Precursor decomposition happens on a gold surface; however, it does not on a silicon oxide surface. Using a co-reactant it is possible to deposit gold on an oxide surface, indicating that the precursor is present on the surface after an exposure. This raises the question whether the precursor is physisorbed or chemisorbed on the surface and what are the possible nucleation sites on the surface. The adsorption of Me_3AuPMe_3 on high surface area silica at 100°C was studied previously by Pallister and Barry using solid-state NMR spectroscopy measurements. [34] They found that after the Me_3AuPMe_3 exposure several surface species were present, including $AuPMe_3$, reduced gold phosphine, methylated phosphoxides, and graphitic carbon. The precursor preferentially reacts with lone silanol groups and an overall precursor coverage of 10% of the surface is observed. Here, we will discuss *in-situ* transmission FTIR experiments to provide additional data of the nucleation sites of the Me_3AuPMe_3 precursor on a silicon oxide surface.

To study the nucleation stage of the Me_3AuPMe_3 - H_2 plasma ALD process, we performed *in-situ* transmission absorption infrared measurements on double polished silicon substrates, with native oxide. IR measurements were performed during the first 40 ALD cycles of the process. An oxygen plasma pre-treatment was used to remove carbon contamination from the substrate and a substrate temperature of 90°C was used during the deposition.

When the sample was mounted with the surface normal parallel to the incident IR beam there was no visible difference in absorption that can be attributed to the ALD process, see Supporting Information. However, mounting the sample with the surface normal at an angle of 75° with respect to the incident IR beam resulted in noticeable absorption modes from the precursor ligands. This angle lies close to the Brewster angle for silicon in the wavelength region of $2,5\,\mu$m to $25\,\mu$m, i.e. 73.8° assuming a refractive index of 3,44. The transmitted IR beam will therefore be partially P-polarized, indicating that the vibration modes of the precursor ligands are preferentially oriented out of plane. The difference spectra for the first four ALD cycles are displayed in Figure 8.

After the first precursor exposure, there is absorption at 960 cm^{-1}, originating from the PMe_3 ligand of the precursor. This indicates that chemisorption of the precursor occurs during the first exposure. In addition, isolated Si-OH groups (at 3745 cm^{-1}) are consumed during the precursor exposure of the first three ALD cycles. [35]

After the first H_2 plasma there is a shift in absorption from 3745 cm^{-1} to 3680 cm^{-1}. The vibration mode at 3680 cm^{-1} can be linked to hydrogen bonded Si-OH groups. [35] In addition, two broad absorption features appear in the region of 2400 cm^{-1} to

View Article Online
DOI: 10.1039/C9CP06855D

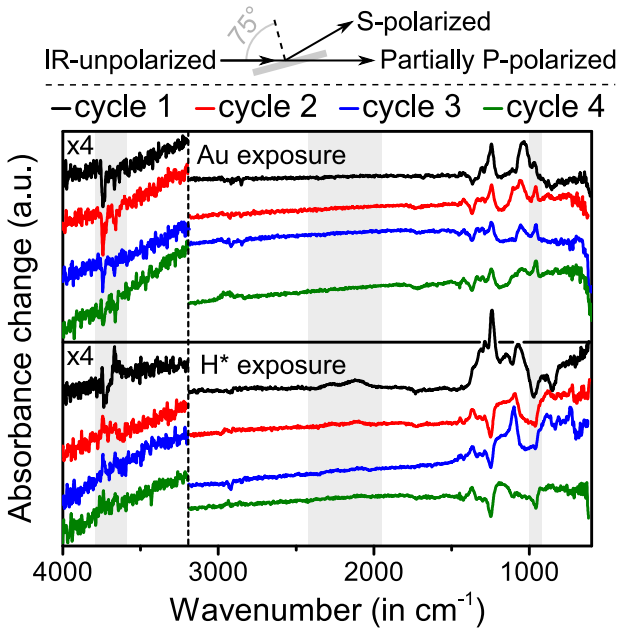

Fig. 8 Transmission difference spectra of the ALD process on a silicon (native oxide) substrate. The substrate temperature was 90°C during this experiment. The angle between the surface normal of the substrate and the incident beam was 75°. A schematic representation of the geometry is drawn above the image. The grey box on the left marks the OH stretching region, which is multiplied by a factor of 4. The middle box marks the Si-H stretching region and the box on the right marks the main PMe_3 deformation mode (at 960 cm^{-1}).

1950 cm^{-1}. Absorption due to the stretching mode of metal-hydrogen bonds is expected to occur in this region. These two features most likely originate from Si-H species that are formed during the H_2 plasma exposure.[36] This suggests that the first H_2 exposure is able to break some of the surface Si-O-Si bonds and forms Si-OH and Si-H species.[37] The following gold exposures also consume a fraction of the Si-OH groups that are present, but this effect stops after the fourth ALD cycle. This indicates that these groups are mainly consumed during the initial nucleation stage. After several cycles the obtained difference spectra start to resemble the steady growth spectra that were recorded in RAIRS mode on a gold seed layer (Figure 2 and see Supporting Information). These results are in agreement with the results obtained by Pallister and Barry, as they also observed that the Me_3AuPMe_3 has a preference for lone silanol groups as reactive sites on the surface.[34]

3.6 Comparison of Me_3AuPMe_3-based PE-ALD processes with different co-reactants

Currently, two Me_3AuPMe_3-based gold ALD processes have been reported.[1,3] Up till now we have only presented results for the H_2 plasma process, neglecting the existing Me_3AuPMe_3 - O_2 plasma - H_2O ALD process reported by Griffiths et al.[1] However, it is noteworthy that applying the 3-step process with O_2 plasma and H_2O in our pump-type reactor did not result in the reproducible formation of metallic gold, but rather in the growth of an amorphous gold containing film.

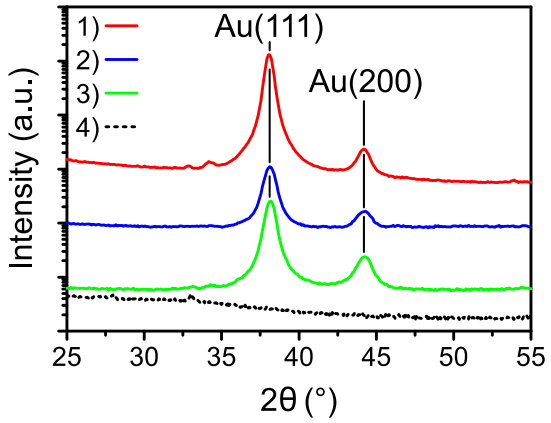

Fig. 9 XRD patterns of four ALD deposited gold films on silicon (native oxide), all depositions were performed at a substrate temperature of 120°C. The Au(111) and Au(200) peaks are respectively marked at 38.3° and 44.5°. 1) Me_3AuPMe_3 - H_2 plasma process, performed in a pump-type reactor (equivalent to 21 nm of sputtered gold). 2) Me_3AuPMe_3 - O_2 plasma - H_2 plasma process, performed in a pump-type reactor (equivalent to 6 nm of sputtered gold). 3) a Me_3AuPMe_3 - O_2 plasma - H_2O process, performed in a flow-type reactor (equivalent to 9 nm of sputtered gold). 4) a Me_3AuPMe_3 - O_2 plasma - H_2O process, performed in a pump-type reactor (equivalent to 10 nm of sputtered gold). The displayed patterns were given an offset.

By swapping the H_2O exposure in the three-step process by a H_2 plasma (Me_3AuPMe_3 - O_2* - H_2*) it was possible to deposit metallic gold films. XRD patterns for the above mentioned deposition processes (H_2*, O_2*-H_2O, O_2*-H_2* in pump-type) are shown in Figure 9, together with a reference of a sample grown by the O_2*-H_2O process in a flow-type reactor. The patterns indicate that the only process that does not yield crystalline gold films is the Me_3AuPMe_3 - O_2 plasma - H_2O process performed in a pump-type reactor, in contrast to the same process applied in a flow-type reactor. The other films show diffraction peaks for Au(111) and Au(200) planes, proving their crystalline nature.

XPS measurements were also performed on these samples, the measured O1s, C1s, P2p, and Au4f peaks on the air-exposed surface and after 100 seconds of argon sputtering are displayed in Figure 10. For all samples there is adventitious carbon present on the surface, but no carbon is present in the film itself. The Au4f peaks are not in a pure metallic state for the Me_3AuPMe_3 - O_2 plasma - H_2O process in a pump-type reactor showing gold in a Au(0) and Au(+1) oxidation state. After sputtering the Au4f peaks are of a metallic nature, however it is most likely that the Au(+1) species are reduced to Au(0) as a consequence of the sputtering process and as such this cannot be taken as an indication that the underlying gold is in a metallic state, which would otherwise conflict with the observed XRD pattern of this film (Figure 9). The gold in the other three samples is in a metallic state, as deposited and after sputtering, which is in agreement with the measured XRD patterns (Figure 9). On all samples there is a O1s peak visible, which for the Me_3AuPMe_3 - O_2 plasma - H_2O flow-type process and for the Me_3AuPMe_3 - H_2 plasma process has a binding energy around 532,9 eV and most likely originates from the silicon oxide of the substrate. For these two samples, there

View Article Online
DOI: 10.1039/C9CP06855D

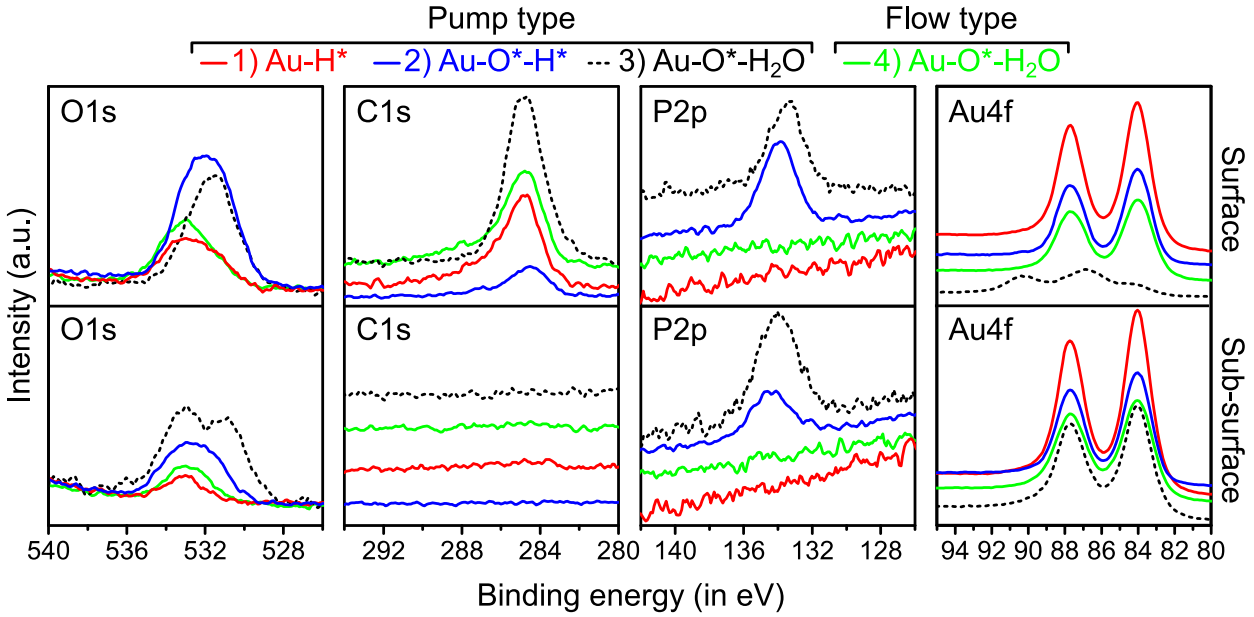

Fig. 10 XPS spectra of four gold films on silicon (native oxide) substrates for the air-exposed samples (top panels) and after removal of the top surface by argon sputtering (bottom panels). 1) a Me_3AuPMe_3 - H_2 plasma process, performed in a pump-type reactor (equivalent to 21 nm of sputtered gold). 2) a Me_3AuPMe_3 - O_2 plasma - H_2 plasma process, performed in a pump-type reactor (equivalent to 6 nm of sputtered gold). 3) a Me_3AuPMe_3 - O_2 plasma - H_2O process, performed in a flow-type reactor (equivalent to 9 nm of sputtered gold). 4) a Me_3AuPMe_3 - O_2 plasma - H_2O process, performed in a pump-type reactor (equivalent to 10 nm of sputtered gold). The displayed spectra were given an offset.

is also no phosphorous present on the surface or after sputtering, showing that these films consist of pure gold. For the other two samples, there is a clear presence of phosphorous, both on the surface and after sputtering. The P2p peaks have a binding energy between 133,5 eV and 134,6 eV, which is consistent with P-O and P=O bonds, originating from phosphate groups.[38,39] These results show that pure gold films can be deposited in a flow-type reactor using O_2 plasma and H_2O as co-reactants and in a pump-type reactor when using H_2 plasma. In a pump-type reactor, the use of an O_2 plasma results in the formation of a gold containing phosphate layer, and reducing the deposited layer to metallic gold is not possible using H_2O but can be achieved when using H_2 plasma as the second co-reactant. However, even the use of H_2 plasma is not able to easily remove the phosphate layer that is formed during the O_2 plasma exposure. It is possible that a difference in pressure for the used H_2O exposure between both reactor types leads to the incomplete removal of the phosphate layer, with a maximum H_2O partial pressure of 0,17 mbar in the flow-type reactor. For this reason, the used pressure during the H_2O exposure was varied between $5x10^{-3}$ mbar and 5 mbar; however, there was no difference in the gold-phosphate films that were formed in these experiments. It is possible that hydrogenating the phosphate layer to from phosphoric acid is followed by dehydrogenation in a pump-type reactor, instead of removing it from the surface. Another, more likely, possibility is that differences in the O_2 plasma properties that are used during the process lead to significantly different phosphate layers, making it more difficult to remove from the surface with a water exposure in a pump-type system.

Depositions using the Me_3AuPMe_3 - O_2 plasma - H_2O process in our pump-type reactors always yielded amorphous gold containing phosphate films, which is a clear difference compared to the results obtained for this process in a flow-type reactor.

4 Conclusion

The reaction mechanism and ligand stability of the Me_3AuPMe_3 - H_2 plasma process in the steady growth regime has been investigated in a pump-type reactor. During the main reaction mechanism, the PMe_3 and CH_3 ligands of the precursor remain on the gold surface after chemisorption of the Me_3AuPMe_3 molecules, causing self-saturating behaviour during the precursor exposure. The ligands are removed by the H_2 plasma exposure, resulting in the formation of CH_4 and possibly (tri,di)methylphosphine/phosphine groups.

A minor fraction of precursor decomposition occurs due to the desorption of the ligands from the surface, as this effect creates additional adsorption sites for the next precursor exposure in a decomposition experiment. For substrate temperatures above 100°C the amount of precursor decomposition increases with substrate temperature and at 120°C the decomposition becomes larger than the GPC of the ALD process. At this temperature the deposition occurs through CVD as there is no self-limiting behaviour of the surface during the precursor exposure. At all substrate temperatures the CH_3 groups get removed from the surface over time, most likely in the form of CH_4. This occurs faster at higher substrate temperatures. The desorption of the PMe_3 groups from the surface, which increases with temperature, seems to be the main factor that determines the precursor decomposition behaviour.

Importantly, precursor decomposition does not occur on a SiO_2

View Article Online
DOI: 10.1039/C9CP06855D

surface, hence another reaction mechanism must be responsible for the nucleation of Au PE-ALD on this surface. Transmission IR measurements on SiO_2 substrates indicate that Si-OH surface groups are consumed during the initial Me_3AuPMe_3 exposures, which makes them the most likely candidates to act as nucleation sites for the Me_3AuPMe_3 - H_2 plasma process. This observation is in agreement with the results of Pallister and Barry of the adsorption of Me_3AuPMe_3 on high surface area silica powder.[34]

Finally, we used O_2 plasma and H_2O as co-reactants in our pump-type ALD systems and compared the obtained film to a metallic and chemically pure gold film that was deposited in a commercial flow-type reactor, using the Me_3AuPMe_3 - O_2 plasma - H_2O gold ALD process.[1] Instead of a metallic gold film we obtained amorphous gold-containing phosphate films, as verified by XPS and XRD measurements. Swapping the H_2O exposure step with a H_2 plasma resulted in the formation of metallic gold films, showing that a stronger reducing co-reactant is required in pump-type systems. However, the use of a H_2 plasma in the process was not sufficient to completely remove the phosphate layer that is formed during the O_2 plasma step. This indicates that, once formed, it is difficult to remove the phosphate layer in a pump-type ALD system, where the Me_3AuPMe_3 - H_2 plasma two step process is the preferred process for obtaining high quality gold films.

Conflicts of interest

There are no conflicts of interest to declare

Acknowledgement

This research was funded by FWO-Vlaanderen and the Flemish Government (Medium-scale research infrastructure funding, Hercules funding). M.M.M. and J.D. received financial support through a personal FWO research grant. J.D. also received funding through the FWO "Krediet aan Navorsers" (1527916N).

Notes and references

1 M. B. E. Griffiths, P. J. Pallister, D. J. Mandia and S. T. Barry, *Chemistry of Materials*, 2016, **28**, 44–46.
2 M. Mäkelä, T. Hatanpää, K. Mizohata, J. Räisänen, M. Ritala and M. Leskelä, *Chemistry of Materials*, 2017, **29**, 6130–6136.
3 M. Van Daele, M. B. E. Griffiths, A. Raza, M. M. Minjauw, E. Solano, J.-Y. Feng, R. K. Ramachandran, S. Clemmen, R. Baets, S. T. Barry, C. Detavernier and J. Dendooven, *ACS Applied Materials & Interfaces*, 2019, **11**, 37229–37238.
4 T. Basova, A. Hassan and N. Morozova, *Coordination Chemistry Reviews*, 2019, **380**, 58 – 82.
5 G. E. Coates and C. Parkin, *J. Chem. Soc.*, 1963, 421–429.
6 A. Tamaki and J. Kochi, *Journal of Organometallic Chemistry*, 1973, **61**, 441 – 450.
7 S. Komiya, T. A. Albright, R. Hoffmann and J. K. Kochi, *Journal of the American Chemical Society*, 1976, **98**, 7255–7265.
8 S. Komiya and J. K. Kochi, *Journal of the American Chemical Society*, 1976, **98**, 7599–7607.
9 J. L. Davidson, P. John, P. G. Roberts, M. G. Jubber and J. I. B. Wilson, *Chemistry of Materials*, 1994, **6**, 1712–1718.
10 C. F. Shaw and R. S. Tobias, *Inorganic Chemistry*, 1973, **12**, 965–978.
11 M. Van Daele, C. Detavernier and J. Dendooven, *Phys. Chem. Chem. Phys.*, 2018, **20**, 25343–25356.
12 M. M. Minjauw, H. Rijckaert, I. V. Driessche, C. Detavernier and J. Dendooven, *Chemistry of Materials*, 2019, **31**, 1491–1499.
13 H.-G. Cho and L. Andrews, *Organometallics*, 2013, **32**, 2753–2759.
14 C. F. Shaw and R. S. Tobias, *Inorganic Chemistry*, 1973, **12**, 965–978.
15 D. C. McKean, G. P. McQuillan, W. F. Murphy and F. Zerbetto, *The Journal of Physical Chemistry*, 1990, **94**, 4820–4831.
16 X. Wang and L. Andrews, *The Journal of Physical Chemistry A*, 2002, **106**, 3744–3748.
17 M. Haruta, *Catalysis Today*, 1997, **36**, 153 – 166.
18 L. Stobiński and R. Duś, *Surface Science*, 1993, **298**, 101 – 106.
19 H. Kariis, G. Westermark, I. Persson and B. Liedberg, *Langmuir*, 1998, **14**, 2736–2743.
20 K. Uvdal, I. Persson and B. Liedberg, *Langmuir*, 1995, **11**, 1252–1256.
21 U. B. Steiner, P. Neuenschwander, W. R. Caseri, U. W. Suter and F. Stucki, *Langmuir*, 1992, **8**, 90–94.
22 G. Westermark, H. Kariis, I. Persson and B. Liedberg, *Colloids and Surfaces A: Physicochemical and Engineering Aspects*, 1999, **150**, 31 – 43.
23 A. D. Jewell, H. L. Tierney and E. C. H. Sykes, *Phys. Rev. B*, 2010, **82**, 205401.
24 M. B. E. Griffiths, S. E. Koponen, D. J. Mandia, J. F. McLeod, J. P. Coyle, J. J. Sims, J. B. Giorgi, E. R. Sirianni, G. P. A. Yap and S. T. Barry, *Chemistry of Materials*, 2015, **27**, 6116–6124.
25 A. J. M. Mackus, N. Leick, L. Baker and W. M. M. Kessels, *Chemistry of Materials*, 2012, **24**, 1752–1761.
26 F.-X. Li and P. B. Armentrout, *The Journal of Chemical Physics*, 2006, **125**, 133114.
27 S. M. Lang, T. M. Bernhardt, R. N. Barnett and U. Landman, *ChemPhysChem*, 2010, **11**, 1570–1577.
28 S. M. Lang, T. M. Bernhardt, R. N. Barnett and U. Landman, *The Journal of Physical Chemistry C*, 2011, **115**, 6788–6795.
29 S. Lang, T. Bernhardt, R. Barnett and U. Landman, *Angewandte Chemie International Edition*, 2010, **49**, 980–983.
30 S. M. Lang, T. M. Bernhardt, V. Chernyy, J. M. Bakker, R. N. Barnett and U. Landman, *Angewandte Chemie International Edition*, 2017, **56**, 13406–13410.
31 D. M. Cox, R. Brickman, K. Creegan and A. Kaldor, *Zeitschrift für Physik D Atoms, Molecules and Clusters*, 1991, **19**, 353–355.
32 A. Paul, M. X. Yang and B. E. Bent, *Surface Science*, 1993, **297**, 327 – 344.
33 A. Paul and B. Bent, *Journal of Catalysis*, 1994, **147**, 264 – 271.
34 P. J. Pallister and S. T. Barry, *The Journal of Chemical Physics*, 2017, **146**, 052812.

View Article Online
DOI: 10.1039/C9CP06855D

35 P. Gupta, A. Dillon, A. Bracker and S. George, *Surface Science*, 1991, **245**, 360 – 372.

36 A. V. Rao, F. Ozanam and J. N. Chazalviel, *Journal of The Electrochemical Society*, 1991, **138**, 153–159.

37 S. Qin, J. D. Bernstein and C. Chan, *Journal of Electronic Materials*, 1996, **25**, 507 – 511.

38 E. Onyiriuka, *Journal of Non-Crystalline Solids*, 1993, **163**, 268 – 273.

39 M. T. Edmonds, A. Tadich, A. Carvalho, A. Ziletti, K. M. O'Donnell, S. P. Koenig, D. F. Coker, B. Özyilmaz, A. H. C. Neto and M. S. Fuhrer, *ACS Applied Materials & Interfaces*, 2015, **7**, 14557–14562.

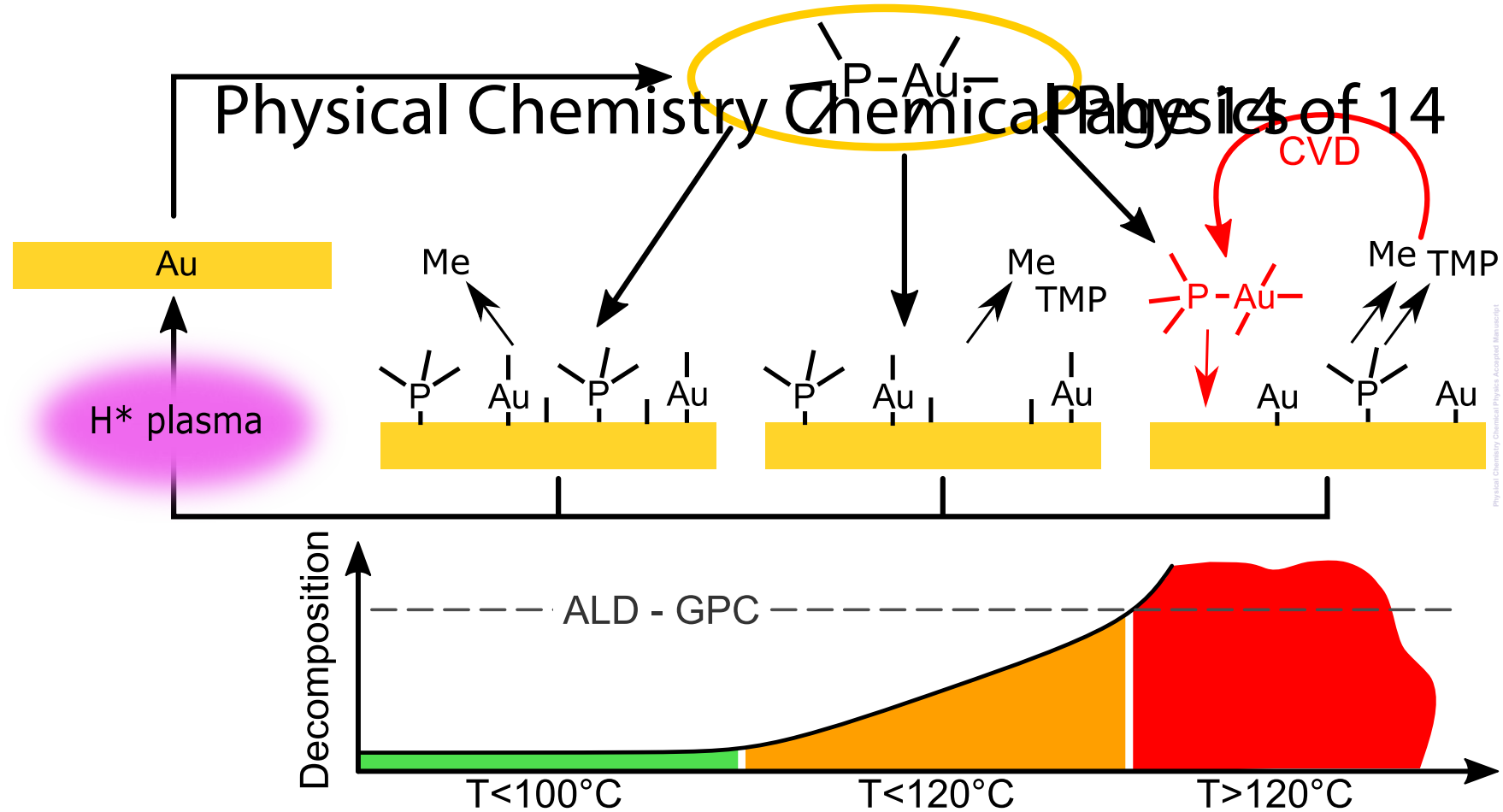
P-Au
Au
H* plasma
Me
TMP
P
Au
CVD
Decomposition
ALD - GPC
T<100°C
T<120°C
T>120°C